

SLS Symposium on Fluids and Soft Matter

Tuesday, September 3, 2013

10:00 to 12:15, WBGB/019

10:00 Nanostructured Light-Responsive Polymer Brushes

Matthias Dübner, Nicholas D. Spencer, Celestino Padeste

10:30 Hydration forces and ion-ion correlation in confined fluids revealed by X-ray Reflectivity

S. Liuzzi, S. Chodankar, R.M. Espinosa Marzal, M. Guizar-Sicairos, A. Diaz, M. Heuberger and J. Friso van der Veen

11:00 Coffee

11:15 Gas-Phase Decomposition of Formic Acid on Supported Metal Catalysts

A. Beloqui Redondo, M. A. Brown, and J. A. van Bokhoven

11:45 Phase contrast mammography: A novel tool for breast cancer screening and diagnosis

Z. Wang, N. Hauser, R. A. Kubik-Huch, G. Singer, E. Roessl, T. Köhler, U. van Stevendaal, N. Wieberneit, and M. Stampanoni

Nanostructured Light-Responsive Polymer Brushes

Matthias Dübner^{1,2}, Nicholas D. Spencer², Celestino Padeste¹

¹ Laboratory for Micro- and Nanotechnology, Paul Scherrer Institut, CH-5232 Villigen PSI, Switzerland; matthias.duebner@psi.ch, www.psi.ch/lmn

² Laboratory for Surface Science and Technology, Department of Materials, ETH Zürich, CH-8093 Zürich, Switzerland

ABSTRACT

Light-induced reversible switching of surface properties enables the creation of remote-controlled smart surfaces. The aim of this work is the growth of nano-patterned photo-responsive polymer brushes which allow the investigation of switching phenomena at a molecular level. We demonstrate different strategies to form photochromic spiropyran-containing polymer brushes, on poly-(ethylene-*alt*-tetrafluoroethylene) (ETFE) surfaces via post-modification. Brushes of poly-(vinyl amine) (PVAm) or poly-(glycidyl methacrylate) (PGMA) are grafted from the surface of 100 μm thick ETFE foils by free-radical polymerization (FRP). Patterns of radicals serving as initiators are created by exposure to EUV-light using the X-ray interference lithography (XIL-II) beamline at the Swiss Light Source (SLS). Depending on the diffraction mask used, various periodic brush structures with resolution in the micrometer to nanometer scale can be produced.^[i, ii, iii] spiropyran moieties are covalently bound in a second step to previously grafted PGMA or PVAm brush structures.

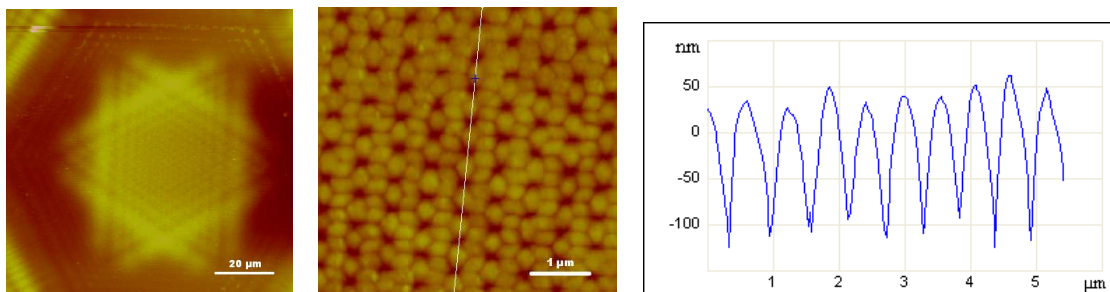


Figure 01: AFM images (a, b) and cross-section (c) of a PGMA nanostructure. The structure was defined by 6 interfering EUV-beams. Structure dimensions: width = 450 nm, height = 150 nm.

ⁱ H.-P. Brack, C. Padeste, M. Slaski, S. Alkan, H.H. Solak, *JACS*, **2004**, 126, 4, 1004-1005.

ⁱⁱ S. Neuhaus, C. Padeste, H.H. Solak, N.D. Spencer, *Polymer* **2010**, 51, 4037.

ⁱⁱⁱ P. Farquet, C. Padeste, H.H. Solak, S.A. Gürsel, G.G. Scherrer, A. Wokaun, *Macromolecules* **2008**, 41, 17, 6309-6316.

Hydration forces and ion-ion correlation in confined fluids revealed by X-ray Reflectivity

S. Liuzzi¹, S. Chodankar¹, R.M. Espinosa Marzal², M. Guizar-Sicairos¹, A. Diaz¹, M. Heuberger^{2,3} and J. Friso van der Veen^{1,2}

¹ Paul Scherrer Institut, 5232, Villigen PSI, Switzerland

² ETH Zürich, 8093 Zürich, Switzerland

³ EMPA, 9014 St. Gallen, Switzerland

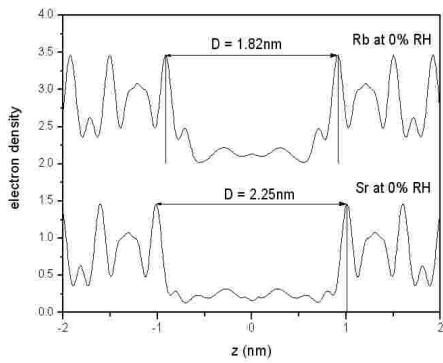
When a liquid is confined within a nanometer-sized gap, the combination of interfacial effects and size often confer to the system properties much different from those observed in bulk fluids [1]. In particular, understanding the structure of electrolytes confined between two aluminium-phyllsilicates walls could be enlightening in a number of fields, ranging from biology to nuclear waste management, as well as clarify some fundamental issues regarding alkali hydration energies and their influence on the surrounding hydrogen bond network.

We have adapted a surface force apparatus (SFA) [2] to be used as confinement device for two sets of X-ray reflectivity (XRR) experiments conducted at the cSAXS (XSA12) beamline of the Swiss Light Source at PSI. A pair of cylinder-shaped muscovite mica membranes were made to approach each other until a flat contact area was formed. We have then performed XRR experiments from the contact area as a function of the momentum transfer q ranging from 0 to 3.5 \AA^{-1} (extended to 7 \AA^{-1} for the second set). Model dependent fits [3] to the measured reflectivity $I(q)$ allowed us to determine the minimum gap distance and the electron density profile along the confinement direction [4].

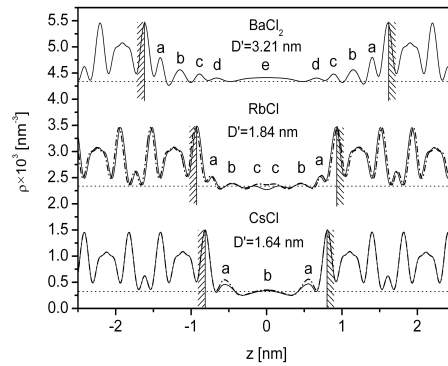
In the first set of experiments, the natural layer of K^+ ions present on cleaved mica surfaces was substituted with monovalent Rb^+ or divalent Sr^{2+} ions. The ion-exchanged membranes were brought into contact in a nitrogen environment with controlled relative humidity (RH). XRR measurements were then made at 0 and 60 % RH.

In the second set droplets of RbCl , CsCl and BaCl_2 solutions at different concentrations were confined. To achieve such confinement, we had to screen out the double layer repulsion and allow attraction between the mica membranes by working at high concentrations with Debye length $\lambda_D < 1 \text{ nm}$.

We have quantitatively determined the minimum gap distance between the mica surfaces at $\sim 10^5 \text{ Pa}$ applied pressure under the influence of different surface ions and electrolytes. In all cases we have observed layered electron density profiles within the gap, with the layering generally being stronger for more strongly correlated systems. A comparison between confined chloride solutions with different monovalent and divalent cations (Cs^+ , Rb^+ and Ba^{2+}) reveals cation specific effects which can be related to concentration, ion size and hydration behavior. For example, we observe characteristic differences between the relative proportions of hydrated inner- and outer-sphere species and in the coverages of the inner membrane surfaces by directly adsorbed ions. Moreover, ordering in strongly correlated BaCl_2 is interpreted as alternate cation-anion layering. Structure models for the measured density profiles will be presented and discussed.



(i)



(ii)

Figure: Electron density in the confined gap for (i) Rb and Sr ion exchanged mica surfaces at 0 % RH and (ii) BaCl₂, RbCl and CsCl at 1.7, 7.5, 5.0, 11 and 6 m, respectively.

Bibliography

1. Israelachvili, J.N., Intermolecular and surface forces: revised third edition. 2011: Academic press.
2. Perret, E., et al., Molecular liquid under nanometre confinement: density profiles underlying oscillatory forces. *Journal of Physics: Condensed Matter*, 2010. 22(23): p. 235102.
3. Perret, E., et al., X-ray reflectivity theory for determining the density profile of a liquid under nanometre confinement. *Journal of synchrotron radiation*, 2010. 17(4): p. 465-472.
4. Chodankar, S., et al., Density profile of water in nanoslit. *EPL (Europhysics Letters)*, 2012. 99(2): p. 26001.

Gas-Phase Decomposition of Formic Acid on Supported Metal Catalysts

A. Beloqui Redondo,^a M. A. Brown,^a and J. A. van Bokhoven^{a,b}

^aInstitute for Chemical and Bioengineering, ETH Zürich, 8093 Zurich, Switzerland

^bLaboratory for Catalysis and Sustainable Chemistry PSI, 5232 Villigen, Switzerland
amaia.beloqui@chem.ethz.ch

The catalytic decomposition of formic acid is recently attracting renewed attention due to the formation of H₂ via reaction (1). A second possible reaction pathway is the production of CO and H₂O, shown in reaction (2).



Other products such as formaldehyde [1], methanol [1] and methane [2] have been reported, however for the most part the study of this reaction is limited to dehydrogenation and dehydration, making it unclear whether their occurrence is monitored or not. Under the assumption that only reactions (1) and (2) are relevant a common way to calculate the selectivity to H₂, S_{H₂}, is by setting it equal to the selectivity to CO₂, as in Eq. (3)

$$S_{\text{H}_2} = S_{\text{CO}_2} = \frac{[\text{CO}_2]}{[\text{CO}_2] + [\text{CO}]} \quad (3)$$

where [CO₂] and [CO] are the concentrations of CO₂ and CO, respectively.

An experimental setup based on gas chromatography (GC) has been developed to determine the conversion and selectivity of different metal supported catalysts in the formic acid decomposition directly. The direct calculation of the hydrogen selectivity in Eq. (4) was done by taking into account the hydrogen concentration [H₂], the HCOOH conversion X_{HCOOH} and the normalization factor of the internal standard calibration f_{H₂}. Furthermore, the presence of side products not originating from reactions (1) and (2) was detected with all catalysts.

$$S_{\text{H}_2} = f_{\text{H}_2} \cdot \frac{[\text{H}_2]/[\text{N}_2]}{[\text{HCOOH}]_0 \cdot X_{\text{HCOOH}}} \quad (4)$$

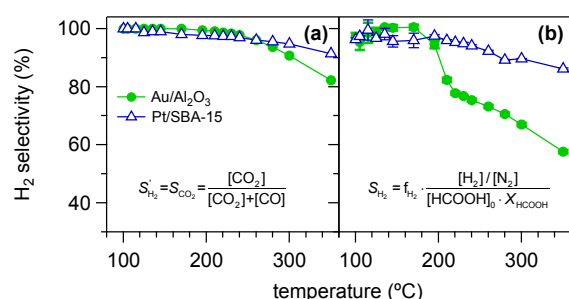


Figure 1. Hydrogen selectivity temperature profiles for Au/Al₂O₃ (green) and Pt/SBA-15 (blue) calculated (a) indirectly with Eq. (3) and (b) directly with Eq. (4).

References

1. Gazsi, A., T. Bánsági, and F. Solymosi, J. Phys. Chem. C 115 (2011) 15459.
2. Bulushev, D.a., S. Beloshapkin, and J.R.H. Ross, Catal. Today 154 (2010) 7.

Phase contrast mammography: A novel tool for breast cancer screening and diagnosis

Z. Wang¹, N. Hauser², R. A. Kubik-Huch³, G. Singer⁴, E. Roessl⁵, T. Köhler⁵, U. van Stevendaal⁵, N. Wieberneit⁶, and M. Stampanoni^{1,7}

¹Swiss Light Source, Paul Scherrer Institut, 5232 Villigen, Switzerland

²Department of Gynecology and Obstetrics, Interdisciplinary Breast Center Baden, Kantonsspital Baden, 5404 Baden, Switzerland

³Department of Radiology, Kantonsspital Baden, 5404 Baden, Switzerland

⁴Institute of Pathology, Kantonsspital Baden, 5404 Baden, Switzerland

⁵Philips Technologie GmbH, Röntgenstrasse 24, 22335 Hamburg, Germany

⁶Philips Healthcare, Imaging Systems, Röntgenstrasse 24, 22335 Hamburg, Germany

⁷Institute for Biomedical Engineering, University and ETH Zürich, 8092 Zürich, Switzerland

Phase contrast mammography using grating interferometer is a promising alternative to current mammography. Preserving the conventional absorption contrast, this novel technology also yields differential phase contrast and small-angle scattering contrast simultaneously. Our research team imaged mastectomy breast samples from 33 patients using this technology and a multicenter, international reader study is performed aiming at the evaluation of its clinical relevance. The results show that phase contrast mammography images have a better image quality with respect to sharpness ($p < 0.001$), lesions delineation ($p < 0.001$), visibility of microcalcifications ($p < 0.001$) and additional clinically relevant information ($p < 0.001$), resulting in a general improvement in image quality.

Additionally, by combining the three complementary signals, quantitative information can be obtained to further improve screening and diagnosis. We proposed a method which is able to discern microcalcification types noninvasively as well as a method for quantitative volumetric breast density estimation. The first one provides a possible way to discern the benign and malignant breast lesions in the imaging stage thereby reducing unnecessary biopsy rate and the second yields more accurate estimation about breast density, which is a strong indicator of breast cancer risk, overcoming the subjectivity of the methods in daily routines.